American Journal of Energy Engineering
2022; 10(2): 45-52
http://www.sciencepublishinggroup.com/j/ajee
doi: 10.11648/j.ajee.20221002.13
ISSN: 2329-1648 (Print); ISSN: 2329-163X (Online)

Performance Investigation of PCM/Pin Fin Coupled Battery Thermal Management System

Xipo Lu[1], Jingtao Jin[1], Wei Kong[1, *], Leitao Han[2]

[1]School of Energy and Power, Jiangsu University of Science and Technology, Zhenjiang, China

[2]State Key Laboratory of Building Safety and Built Environment, Beijing, China

Email address:
wkong@just.edu.cn (Wei Kong)

[*]Corresponding author

To cite this article:
Xipo Lu, Jingtao Jin, Wei Kong, Leitao Han. Performance Investigation of PCM/Pin Fin Coupled Battery Thermal Management System. *American Journal of Energy Engineering*. Vol. 10, No. 2, 2022, pp. 45-52. doi: 10.11648/j.ajee.20221002.13

Received: March 14, 2022; **Accepted**: June 6, 2022; **Published**: June 8, 2022

Abstract: The low thermal conductivity of phase-change materials (PCMs) hampers the commercialization of PCM cooling battery thermal management systems. Further reduction of the thermal resistance between the PCM and batteries is still a challenging problem. In this study, a PCM / pin fin design is proposed. ANSYS Fluent was used to construct the model of PCM / pin fin design. The SIMPLE algorithm and the second-order upwind scheme were used to solve the momentum and energy equations. Compared with the traditional pure PCM and PCM/plate fin designs, the maximum temperature of the battery (T_{max}) was lower for the PCM/pin fin design because the heat transport from the batteries to the PCM was enhanced owing to the pin fin with a larger heat-transfer area. T_{max} for the pure PCM configuration reached 55.76°C after discharge, exceeding the upper-limit temperature of 55°C. In contrast, for the PCM/pin fin design, T_{max} was only 53.44°C. This indicates that the PCM/pin fin design effectively alleviates the heat accumulation of the battery and successfully maintains the battery temperature within a safe range. The effects of PCM thickness and fin section area on thermal behavior were investigated. It was found that the decrease of fin cross-sectional area can significantly reduce T_{max}. When the fin cross-sectional area is 1 mm^2, the T_{max} is only 51.07°C. In addition to control T_{max} under 55°C, the minimum PCM thicknesses were 3.71, 2.89, and 2.38 mm for pure PCM, PCM/plate fin, and PCM/pin fin, respectively. Thus, compared with the other designs, in the PCM/pin fin design, fewer materials are required, the weight of the modules is reduced, and the energy density is improved.

Keywords: Battery Thermal Management Systems, PCM Cooling, Pin Fin, Design

1. Introduction

Electric vehicles (EVs) have become the development trend of the automobile industry. They can be powered by various batteries, such as lead acid batteries, nickel metal hydride batteries, lithium batteries, and fuel cells [1-4]. At present, lithium batteries have considerable advantages with regard to energy density, lifetime, and environmental performance and are the first choice for power batteries [5, 6]. However, EVs are at a high risk of spontaneous combustion owing to the overheating of batteries [7-9]. To avoid the overheating of batteries, battery thermal management systems (BTMSs) have been proposed for controlling the battery temperature [9-11]. The primary objective of a BTMS is to maintain the battery temperature under 55°C [12-14]. When the temperature exceeds 55°C, the capacity of the battery inevitably decreases, sharply reducing the driving range of the EV [14]. Additionally, an excessive temperature difference ($\Delta T > 5$°C) is harmful for batteries [12, 15]. The cycle life of batteries may even be reduced to half for a 2°C increase in ΔT [16]. Therefore, maintaining a temperature difference of less than 5°C is another objective of the BTMS.

PCM cooling has attracted considerable interest in recent years because a large amount of heat can be absorbed during the phase-transition processes of PCMs at a constant

temperature [11, 17]. Compared to air cooling and liquid cooling, the advantages of PCM cooling are apparent, e.g., energy conservation, outstanding temperature uniformity, a relatively low cost, and a simple module (no pump or fan is required) [14, 18-20]. However, PCM cooling is not suitable for high discharge rates, owing to its low thermal conductivity, which hampers its commercialization. There are two main methods for resolving this issue. The first is to prepare new composite materials by mixing high-thermal conductivity fillers with PCMs. Zhang et al. prepared paraffin/expanded graphite (EG) composites and found that with an EG loading fraction of 25%, the thermal conductivity was increased to 10.8 W $m^{-1}°C^{-1}$ [21]. Babapoor et al. used a paraffin/carbon fiber for battery cooling [22]. The results indicated that the battery maximum temperature was reduced by 45%. Qu et al. proposed a novel passive thermal management method using a combination of porous metal foam and a PCM [23]. In addition, to simulate the variable heat transfer of the solid and liquid phases in the porous medium, a thermo-electrochemical coupled model was established. Finally, they proved that the battery temperature can be significantly reduced to the allowable range at a comparatively higher discharge rate by using a PCM with porous metal foam.

The second method involves embedding a metal fin in the PCM to increase the thermal conductivity of the PCM [24]. For cylindrical batteries, Zhang et al. investigated the effects of longitudinal fins and circular fins [25]. The results indicated that both types of fins have certain advantages and disadvantages. Zheng et al. proposed a novel fin structure combining both longitudinal and cylindrical fins [26]. They found that compared to traditional fins, the new fin structure can transfer heat to the PCM more quickly. For prismatic batteries, Wen et al. reported that the maximum temperature of batteries is consistently below 51°C under the condition of 3 C discharge with a PCM/plate fin coupled structure [27].

Although the application of the plate fin reduces the thermal resistance between the PCM and the batteries, there remains a large temperature gradient in the PCM. Hence, further reduction of the thermal resistance between the PCM and the batteries is necessary. In this study, a novel PCM/pin fin BTMS was designed, as shown in Figure 1. Compared to the traditional plate fin, the heat-exchange area between the fin and the PCM was increased when the same fin volume was employed, which improved the heat-dissipation capability of the BTMS [28]. Moreover, numerous studies have confirmed the effectiveness of pin fins for improving the thermal response rate of PCMs and the overall temperature uniformity in other fields [28-31]. Therefore, it is necessary to investigate a PCM/pin fin coupled BTMS.

In this study, PCM/pin fin, PCM/plate fin, and pure PCM models were established using ANSYS Fluent. Subsequently, the performance of the PCM/pin fin, PCM/plate fin, and pure PCM configurations under 5 C discharge was compared. Finally, the effects of the PCM thickness and fin cross-sectional area were examined.

2. Model

2.1. Physical Problem

The PCM cooling system is shown in Figure 1. Numerous prismatic cells were closely placed in this system, and a special heat sink was provided to absorb the heat between two adjacent batteries. The PCM was filled among the fins in the heat sink. Moreover, to evaluate the PCM/pin fin structure rationally, three types of heat sinks were compared in this study. The configuration and dimensions are presented in Figure 2.

In view of the computational load and model symmetry, only a single repeating unit of the system was simulated in this study (marked by the red dotted line in Figure 1(a)). Aluminum was employed as the material of the baseplates and fins owing to its high thermal conductivity and low density. Finally, n-docosane was selected as the PCM considering its 5 C discharge rate. The model parameters are presented in Table 1.

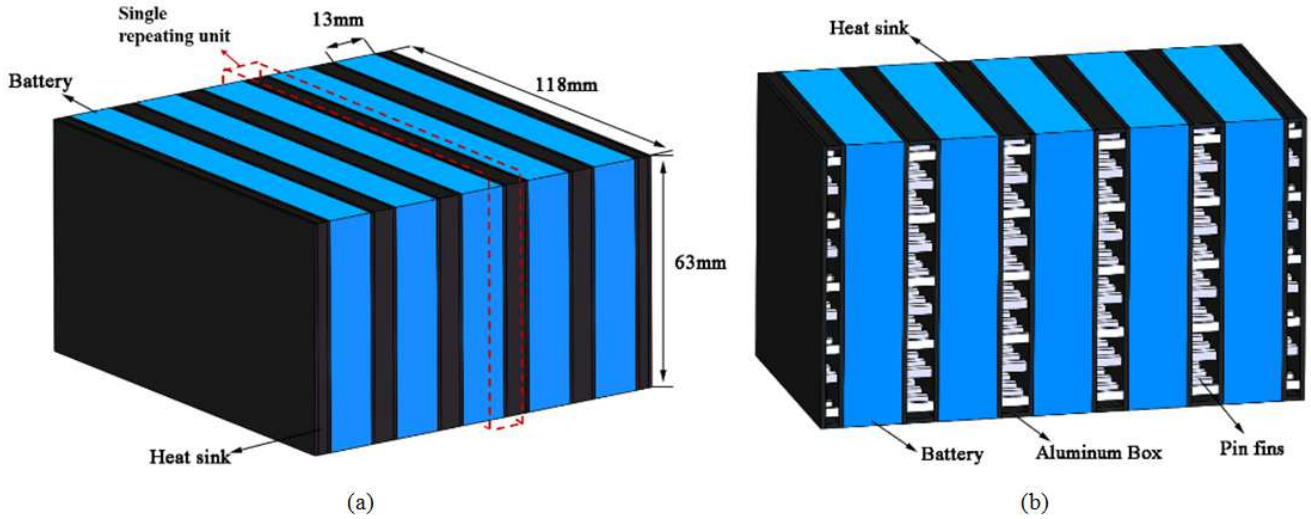

Figure 1. *PCM cooling system: (a) overall view; (b) section view.*

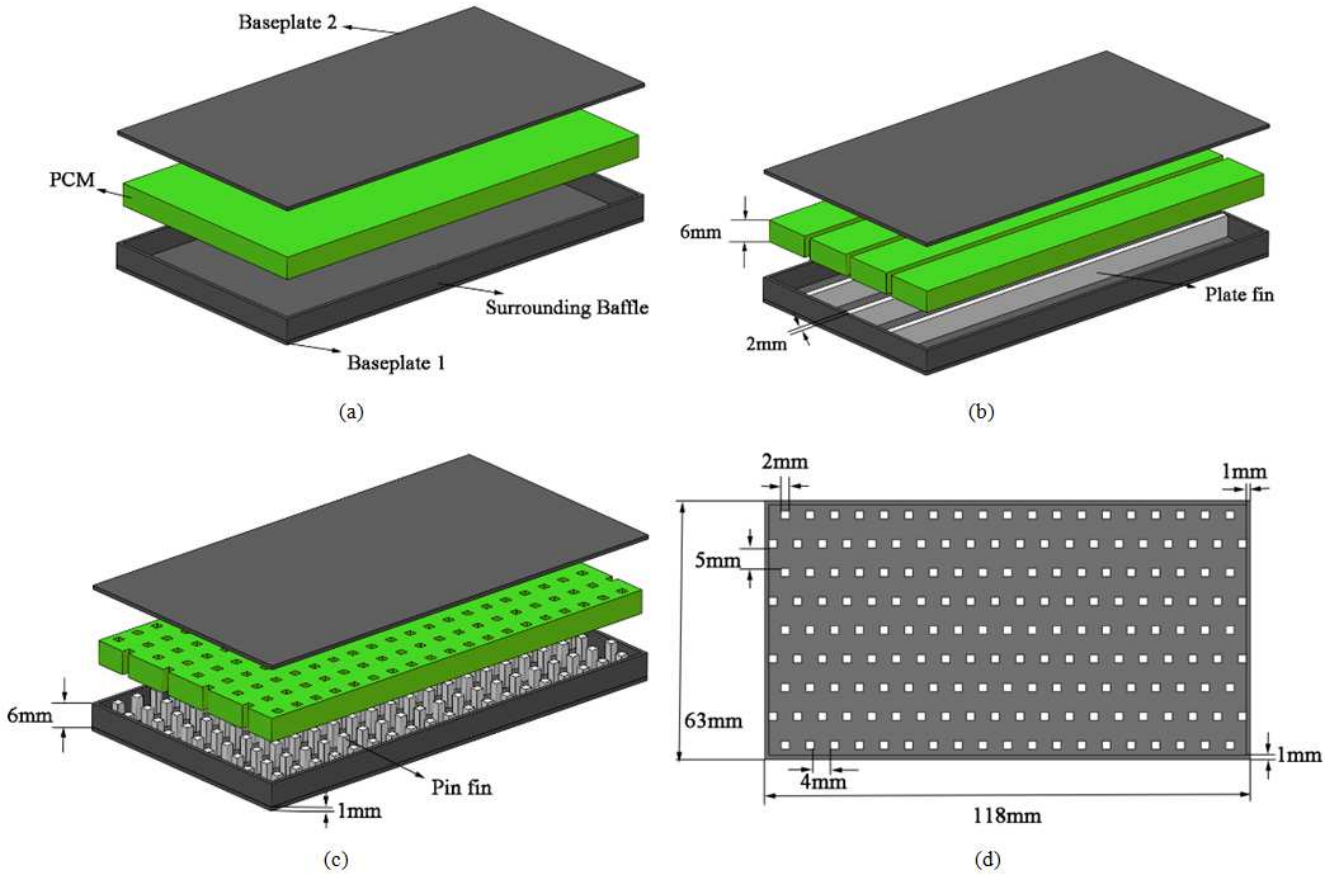

Figure 2. *Schematics of heat sinks: (a) pure PCM; (b) plate fin; (c) pin fin. (d) Detailed dimensions of the pin fin.*

Table 1. *Model parameters [27, 32].*

Parameters	PCM	Battery	Aluminum
Specific heat (J kg^{-1} K^{-1})	2150 (solid) 2275 (liquid)	1108	871
Thermal conductivity (W m^{-1} K^{-1})	0.21 (solid) 0.15 (liquid)	3.9	202.4
Density (kg m^{-3})	791 (solid) 771 (liquid)	2450	2719
Latent heat of PCM (J kg^{-1} K^{-1})	249000		
Melting temperature (°C)	44		
Melting range (°C)	2		
Viscosity of liquid PCM (kg m^{-1} s^{-1})	0.01		

2.2. Governing Equations

The heat transfer in the batteries, fins, and baseplates can be clearly expressed by the energy-conservation equations:

$$\rho_{bat} C_{p,bat} \frac{\partial T}{\partial t} = k_{bat} \nabla^2 T_{bat} + q \tag{1}$$

$$\rho_{fin} C_{p,fin} \frac{\partial T}{\partial t} = k_{fin} \nabla^2 T_{fin} \tag{2}$$

$$\rho_{pla} C_{p,pla} \frac{\partial T}{\partial t} = k_{pla} \nabla^2 T_{pla} \tag{3}$$

where C_p, ρ, and k represent the specific heat capacity, density, and thermal conductivity, respectively, and the subscripts bat, fin, and pla correspond to the battery, fin, and baseplate, respectively. Additionally, q represents the heat source.

For the PCM region, the enthalpy–porosity method is adopted to analyze the heat-transfer process:

$$\frac{\partial(\rho_{pcm} H_{pcm})}{\partial t} + \nabla \cdot (\rho_{pcm} \vec{u} H_{pcm}) = k_{pcm} \nabla^2 T_{pcm} \tag{4}$$

$$H_{pcm} = h_0 + \int_{T_0}^{T} C_{p,pcm} dT + \beta\gamma \tag{5}$$

where ρ_{pcm}, k_{pcm}, T_{pcm}, H_{pcm}, and γ represent the density, thermal conductivity, temperature, enthalpy, and specific latent heat of the PCM, respectively, and h_0 and $C_{p,pcm}$ represent the reference enthalpy and specific heat of PCM, respectively. Because the thermophysical properties of the PCM are largely determined by its state, the liquid fraction

(β) can be given as follows:

$$\begin{cases} \beta=0 & T_{pcm} \le T_s \\ \beta=1 & T_{pcm} \ge T_l \\ \beta=\dfrac{T_{pcm}-T_s}{T_l-T_s} & T_s < T_{pcm} < T_l \end{cases} \tag{6}$$

where T_s and T_l represent the start and end temperatures of the phase transition.

The continuity and momentum equations are used to simulate the natural convection of the PCM after the phase change.

$$\nabla \cdot (\rho \vec{u}) = 0 \tag{7}$$

$$\frac{\partial (\rho \vec{u})}{\partial t} + \nabla \cdot (\rho \vec{u}\vec{u}) = -\nabla p + \nabla \cdot \tau + \rho_\alpha \left[1-\xi(T-T_0)\right]\vec{g} + \frac{(1-\beta)^2}{\beta^2+0.001} A_{mush} \vec{u} \tag{8}$$

Here, τ is the stress tensor, ρ_α represents the density of the PCM at the ambient temperature, and ξ = 0.0008161 K^{-1} and $A_{mush} = 10^5$ are the thermal expansion coefficient of the PCM and the mush zone constant, respectively.

2.3. Boundary Conditions

The initial temperature is 25°C. The boundary conditions between all the components of the module can be expressed as follows:

$$-k_{bat}\frac{\partial T_{bat}}{\partial n} = -k_{pcm}\frac{\partial T_{pcm}}{\partial n} = -k_{fin}\frac{\partial T_{fin}}{\partial n} = -k_{pla}\frac{\partial T_{pla}}{\partial n} \tag{9}$$

The heat flux between the surfaces and the environment can be expressed as follows:

$$-k_s\frac{\partial T_s}{\partial n} = h(T_s - T_0) \tag{10}$$

where h is the convection heat transfer coefficient, whose value is 5 W m^{-2} K^{-1}.

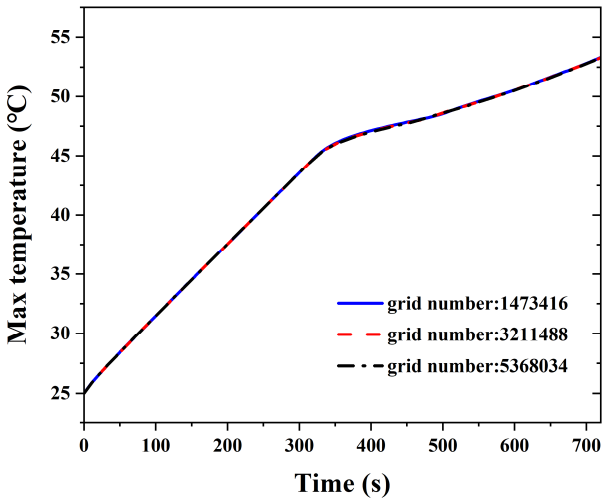

Figure 3. *Verification of grid independence.*

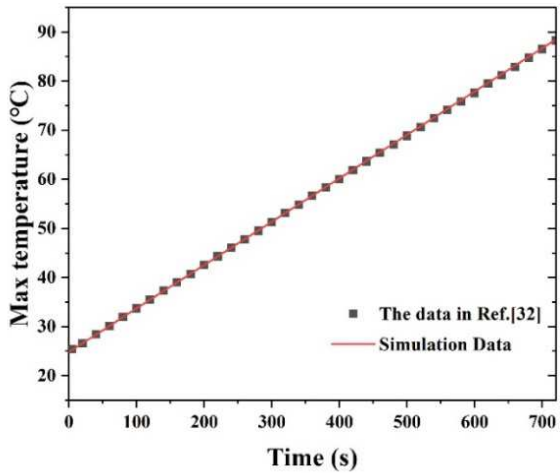

Figure 4. *Validation of the model using the data in Ref. [32]*

2.4. Numerical Implementation

ANSYS Fluent was used to construct the models. The SIMPLE algorithm and the second-order upwind scheme were used to solve the momentum and energy equations. The discharge rate was 5 C, and the heat source was set as 240 kW m^{-3} [32]. Figure 3 shows the verification of grid independence for the PCM/pin fin model. Clearly, a grid number of 1473416 was sufficient for the model. Thus, to reduce the computational cost, the grid number of 1473416 was selected for the calculation in this study. As shown in Figure 4, the maximum temperature (T_{max}) of the battery was consistent with the data reported in Ref. [32], indicating that the model is accurate and creditable.

3. Result and Discussion

3.1. Comparison of Different Configurations

Figure 5 shows the temperature distribution of the battery at the end of the 5 C discharge. Compared to the PCM/plate fin and pure PCM designs, the maximum temperature (T_{max}) for the PCM/pin fin design was lower. This is explained by

the melting situation of the PCM, as shown in Figure 6. The non-uniformity of the PCM melting situation was mainly reflected by two aspects. First, under the effects of the natural convection in the PCM, the upper layer of PCM tended to melt more easily than the lower layer.

Second, the PCM around the metal fin melted more quickly than that elsewhere. For the pure PCM configuration, most of the PCM in the center did not melt because of its low thermal conductivity. However, for the PCM/pin fin configuration, the PCM around the pin fin almost melted because the heat transport from the battery to the PCM was enhanced by the pin fin, which had a better heat-dissipation ability. After discharge, the liquid fractions of PCM for the pure PCM, PCM/plate fin and PCM/pin fin configurations were 61.2%, 73.37%, and 79.21%, respectively, as shown in Figure 7, indicating that the amount of absorbed heat was the largest for the PCM/pin fin design. Tmax for the pure PCM configuration reached 55.76°C after discharge, exceeding the upper-limit temperature of 55°C. In contrast, for the PCM/pin fin design, Tmax was only 53.44°C. This indicates that the PCM/pin fin design effectively alleviates the heat accumulation of the battery and successfully maintains the battery temperature within a safe range.

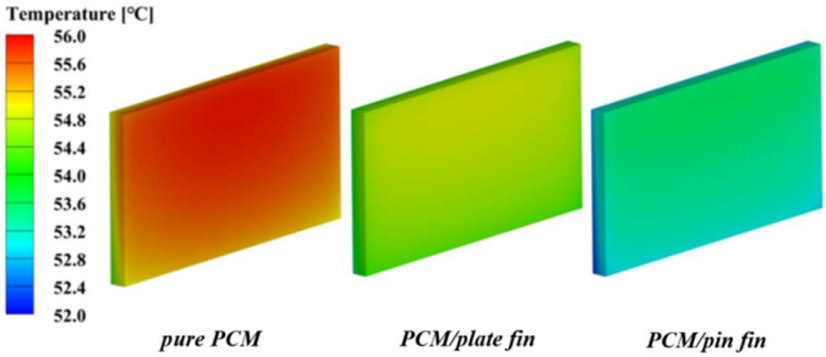

Figure 5. *Temperature distributions of the battery.*

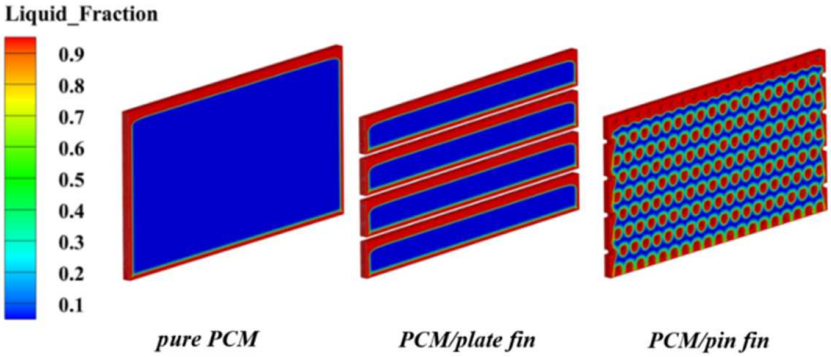

Figure 6. *Liquid fractions of PCM.*

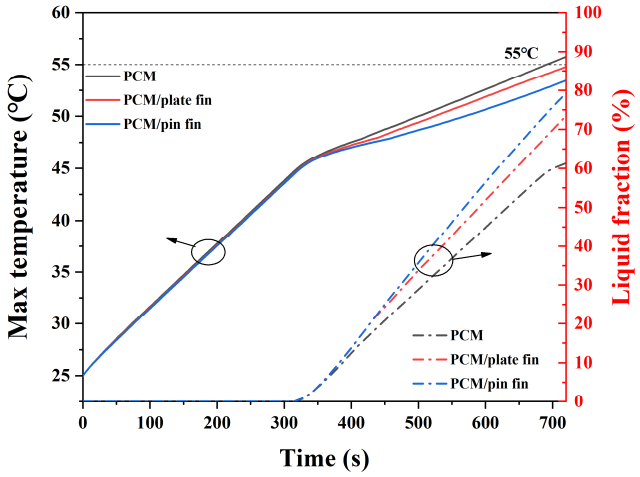

Figure 7. *T_{max} and liquid fraction of PCM with respect to time for different configurations.*

3.2. Effect of PCM Thickness

Figure 8 shows the T_{max} values for different PCM thicknesses at the end of the 5 C discharge. Clearly, the cooling effect of the battery increased with the PCM thickness. For example, when the thickness of the PCM was increased from 2 to 2.5 mm, T_{max} of the PCM/pin fin design decreased by 1.6°C. In addition, for a PCM thickness of 2 mm, T_{max} of the PCM/plate fin design was higher than that of the pure PCM design, whereas for a PCM thickness of 2.5 mm, the opposite was observed. This is explained as follows: on the one hand, adding a plate fin to the PCM facilitated heat transfer between the battery and the PCM; on the other hand, the addition of the plate fin reduced the PCM volume, reducing the capacity for heat absorption. Furthermore, to control T_{max} under 55°C, the minimum PCM thicknesses were 3.71, 2.89, and 2.38 mm, respectively, for the pure PCM, PCM/plate fin, and PCM/pin fin designs. Thus,

compared to the other designs, the PCM/pin fin design saves materials, reduces the weight of the modules, and improves the energy density.

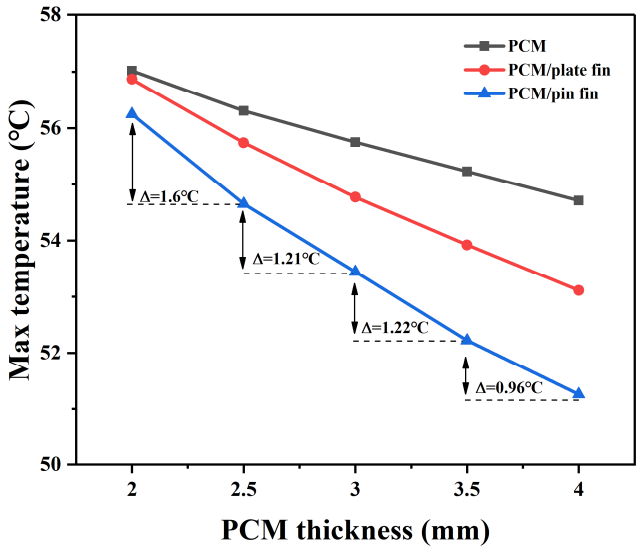

Figure 8. *Effect of the PCM thickness on T_{max}.*

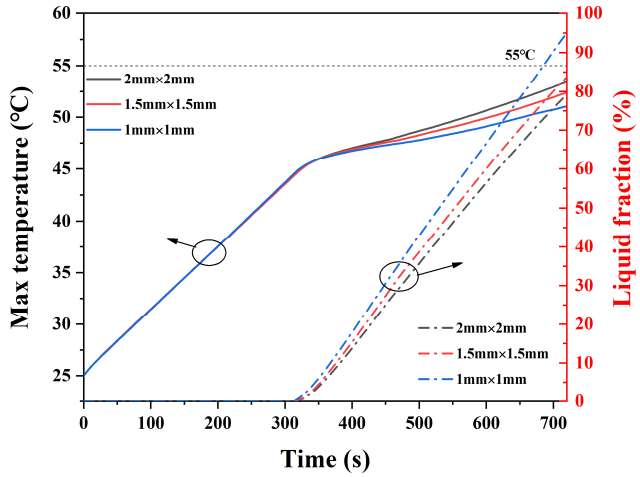

Figure 9. *Effect of the PCM thickness on ΔT.*

3.3. Effect of Pin-Fin Cross-Sectional Area

Figure 10 presents the T_{max} and PCM liquid fraction with respect to time for different fin cross-sectional areas. The total volume fraction of the pin fin was constant (9.36%), and the PCM thickness was 3 mm. As shown in the figure, with a reduction in the fin cross-sectional area, T_{max} decreased, and the liquid fraction of PCM was improved after discharge. This is because when the total volume fraction of the pin fin is fixed, a smaller pin-fin cross-sectional area corresponds to a larger number of pin fins, which is helpful for enhancing the heat transfer in the PCM. In addition, for a fin cross-sectional area of 1 mm^2, T_{max} was only 51.07°C, nearly 4°C below the upper-limit temperature. Thus, reducing T_{max} by decreasing the pin-fin cross-sectional area is an effective approach.

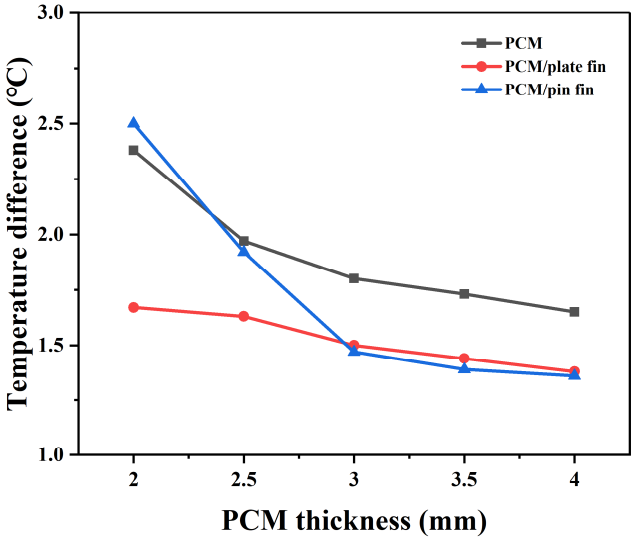

Figure 10. *T_{max} and PCM liquid fraction with respect to time for different fin cross-sectional areas.*

4. Conclusion

Considering that the thermal conductivity of PCMs is too low to satisfy the requirements for a fast response to thermal surges, a novel PCM/pin fin design is proposed to reduce the thermal resistance between a PCM and battery in this study. The effects of the PCM thickness and fin cross-sectional area on the BTMS performance were investigated. The following conclusions were drawn.

1) Compared to the PCM/plate fin and pure PCM designs, the PCM/pin fin design exhibits a superior thermal performance, as it facilitates heat transfer between the battery and the PCM.
2) To control T_{max} under 55°C, the PCM/pin fin design required the smallest PCM thickness among the three designs examined, which saves materials, reduces the weight of the modules, and improves the energy density.
3) A PCM thickness between 3 and 3.5 mm is recommended for the PCM/pin fin design.
4) T_{max} can be effectively reduced by decreasing the pin-fin cross-sectional area.

Due to the limitation of experimental conditions, this paper mainly uses simulation method to study the PCM / pin fin design. It is hoped that the PCM / pin fin design proposed in this paper can be further optimized through experimental methods.

Acknowledgements

This work was financially supported by the National Science Foundation of China (22179054 and 11774324), as well as the Opening Funds of State Key Laboratory of Building Safety and Built Environment & National Engineering Research Center of Building Technology (BSBE2021-14).

References

[1] Li J, Liang M, Cheng W, et al. Life cycle cost of conventional, battery electric, and fuel cell electric vehicles considering traffic and environmental policies in China [J]. International Journal of Hydrogen Energy, 2021, 46 (14): 9553-9566.

[2] Kong W, Han Z, Lu S, et al. A simple but effective design to enhance the performance and durability of direct carbon solid oxide fuel cells [J]. Applied Energy, 2021, 287.

[3] Huang H, Han Z, Lu S, et al. The analysis of structure parameters of MOLB type solid oxide fuel cell [J]. International Journal of Hydrogen Energy, 2020, 45 (39): 20351-20359.

[4] Xiaoling X. Closed-Loop Design for Standalone Photovoltaic-Battery Hybrid Power System [J]. Journal of Electrical and Electronic Engineering, 2016, 4 (5).

[5] Wu B, Xie Y, Meng Y, et al. Construction of unique heterogeneous cobalt–manganese oxide porous microspheres for the assembly of long-cycle and high-rate lithium ion battery anodes [J]. Journal of Materials Chemistry A, 2019, 7 (11): 6149-6160.

[6] Kang Y. Analysis of the Temperature Change of a Single Battery Based on Simulink [J]. International Journal of Electrochemical Science, 2021.

[7] Rani M F H, Razlan Z M, Shahriman A B, et al. Comparative study of surface temperature of lithium-ion polymer cells at different discharging rates by infrared thermography and thermocouple [J]. International Journal of Heat and Mass Transfer, 2020, 153.

[8] Li H. State of Charge Estimation for Lithium-Ion Battery Models Based on a Thermoelectric Coupling Model [J]. International Journal of Electrochemical Science, 2020: 3807-3824.

[9] Nabil T, Helmy Omar A-B, Mohamed Mansour T. Experimental Approach and CFD Simulation of Battery Electric Vehicle Body [J]. International Journal of Fluid Mechanics & Thermal Sciences, 2020, 6 (2).

[10] Yang S. A Review of Lithium-Ion Battery Thermal Management System Strategies and the Evaluate Criteria [J]. International Journal of Electrochemical Science, 2019: 6077-6107.

[11] Rao Z, Wang S. A review of power battery thermal energy management [J]. Renewable and Sustainable Energy Reviews, 2011, 15 (9): 4554-4571.

[12] Wang F, Li T, Fang Y, et al. Heterogeneous structured Mn_2O_3/Fe_2O_3 composite as anode material for high performance lithium ion batteries [J]. Journal of Alloys and Compounds, 2020.

[13] Li H. Electrochemical-thermal coupled model for the optimal design of a liquid cooling module of a cylindrical lithium-ion battery [J]. International Journal of Electrochemical Science, 2021.

[14] Lei S, Shi Y, Chen G. A lithium-ion battery-thermal-management design based on phase-change-material thermal storage and spray cooling [J]. Applied Thermal Engineering, 2020, 168.

[15] Chen F, Wang J, Yang X. Topology optimization design and numerical analysis on cold plates for lithium-ion battery thermal management [J]. International Journal of Heat and Mass Transfer, 2022, 183.

[16] Xia Q, Wang Z, Ren Y, et al. A reliability design method for a lithium-ion battery pack considering the thermal disequilibrium in electric vehicles [J]. Journal of Power Sources, 2018, 386: 10-20.

[17] Nguyen H Q, Shabani B. Thermal management of metal hydride hydrogen storage using phase change materials for standalone solar hydrogen systems: An energy/exergy investigation [J]. International Journal of Hydrogen Energy, 2021.

[18] Du X, Qian Z, Chen Z, et al. Experimental investigation on mini-channel cooling-based thermal management for Li-ion battery module under different cooling schemes [J]. International Journal of Energy Research, 2018, 42 (8): 2781-2788.

[19] Rao Z, Wang S, Zhang G. Simulation and experiment of thermal energy management with phase change material for ageing $LiFePO_4$ power battery [J]. Energy Conversion and Management, 2011, 52 (12): 3408-3414.

[20] Wu W, Wu W, Wang S. Thermal management optimization of a prismatic battery with shape-stabilized phase change material [J]. International Journal of Heat and Mass Transfer, 2018, 121: 967-977.

[21] Ling Z, Chen J, Fang X, et al. Experimental and numerical investigation of the application of phase change materials in a simulative power batteries thermal management system [J]. Applied Energy, 2014, 121: 104-113.

[22] Babapoor A, Azizi M, Karimi G. Thermal management of a Li-ion battery using carbon fiber-PCM composites [J]. Applied Thermal Engineering, 2015, 82: 281-290.

[23] Qu Z G, Li W Q, Tao W Q. Numerical model of the passive thermal management system for high-power lithium ion battery by using porous metal foam saturated with phase change material [J]. International Journal of Hydrogen Energy, 2014, 39 (8): 3904-3913.

[24] Wang Z, Zhang H, Xia X. Experimental investigation on the thermal behavior of cylindrical battery with composite paraffin and fin structure [J]. International Journal of Heat and Mass Transfer, 2017, 109: 958-970.

[25] Weng J, Ouyang D, Yang X, et al. Optimization of the internal fin in a phase-change-material module for battery thermal management [J]. Applied Thermal Engineering, 2020, 167.

[26] Sun Z, Fan R, Yan F, et al. Thermal management of the lithium-ion battery by the composite PCM-Fin structures [J]. International Journal of Heat and Mass Transfer, 2019, 145.

[27] Ping P, Peng R, Kong D, et al. Investigation on thermal management performance of PCM-fin structure for Li-ion battery module in high-temperature environment [J]. Energy Conversion and Management, 2018, 176: 131-146.

[28] Arshad A, Ali H M, Yan W-M, et al. An experimental study of enhanced heat sinks for thermal management using n-eicosane as phase change material [J]. Applied Thermal Engineering, 2018, 132: 52-66.

[29] Ali H M, Ashraf M J, Giovannelli A, et al. Thermal management of electronics: An experimental analysis of triangular, rectangular and circular pin-fin heat sinks for various PCMs [J]. International Journal of Heat and Mass Transfer, 2018, 123: 272-284.

[30] Desai A N, Gunjal A, Singh V K. Numerical investigations of fin efficacy for phase change material (PCM) based thermal control module [J]. International Journal of Heat and Mass Transfer, 2020, 147.

[31] Ren Q, Guo P, Zhu J. Thermal management of electronic devices using pin-fin based cascade microencapsulated PCM/expanded graphite composite [J]. International Journal of Heat and Mass Transfer, 2020, 149.

[32] Rao Z, Wang Q, Huang C. Investigation of the thermal performance of phase change material/mini-channel coupled battery thermal management system [J]. Applied Energy, 2016, 164: 659-669.